Graphene Plasmon Excitation with Ground-State Two-Level Quantum Emitters

Xiaodong Zeng[1,2,*] and M. Suhail Zubairy[2,†]
[1]Department of Physics, Shanghai University, Shanghai 200444, China
[2]Institute for Quantum Science and Engineering (IQSE) and Department of Physics and Astronomy, Texas A&M University, College Station, Texas 77843-4242, USA

(Received 29 April 2020; accepted 22 February 2021; published 16 March 2021)

The transmission of a two-level quantum emitter in its ground state through a graphene nanosheet is investigated. The graphene plasmons (GPs) field distribution, especially the opposite orientations of the vertical electric field components on the two sides of the graphene nanosheet, produces a significant nonadiabatic process during the interaction between the emitter and the localized GPs. By taking into account the counterrotating terms, the excitation of the quantum emitter with simultaneous emission of a GP has a large probability. This happens for emitter speeds of about 10^{-4} times the speed of light. For accelerated emitters, the GPs exhibit thermal field photon distribution with a high temperature. As a consequence, this study provides a promising platform to observe the dynamical Casimir effect as well as a simulation of the Unruh effect.

DOI: 10.1103/PhysRevLett.126.117401

Introduction.—Graphene, a single layer of carbon atoms arranged in a honeycomb lattice, has attracted a lot of interest [1–3]. In particular, the graphene plasmons (GPs) have emerged as a hot topic in recent years due to the strong localization, new frequency range, tunability, and long-lived characteristics [4–11]. The plasmonic wave number can be of the order of $1/\alpha_c$ times the vacuum wave number, where $\alpha_c = 1/137$ is the fine structure constant. This means that the electromagnetic field amplitude has a $(1/\alpha_c)^{3/2} \sim 10^3$ time enhancement leading to a strong coupling with the nearby located quantum emitter. Another remarkable property is that the vertical plasmonic fields on the two sides of the graphene have opposite directions. For a two-level quantum emitter passing through the graphene, the coupling strengths have a sharp flipping, leading to a strong nonadiabatic process.

Nonadiabatic effect, the fast variation of the field in the timescale of the eigenfrequency, is a common phenomenon in quantum mechanics. In quantum electrodynamics, a well-known related effect is the dynamical Casimir effect which describes the conversion of virtual photons into directly observable real photons by a mirror undergoing relativistic motion. This strong nonadiabatic process can be achieved when the physical mirror is moving at a speed close to the speed of light. This is not feasible in a real experiment. This fact has led to a number of alternative proposals, such as using nanomechanical resonators or modulation of the electrical properties of a cavity [12–14].

In this Letter, we propose a realistic experiment to excite the GPs by a quantum emitter initially in the ground state passing through a graphene nanosheet. Compared to dynamical Casimir effect where the mirror should be moving with a speed close to the speed of light c, the required speed in the present scheme is about $10^{-4}c$. This results from the extreme field localization and the direction flipping of the fields on the two sides of the graphene nanosheet. The GPs can be excited with almost unit probability. The energy is conserved in the whole process and can be explained via dynamical Casimir effect. This is in contrast to the earlier methods [12–14] that require analog modulation of the cavity.

It is also interesting to note that the Unruh effect (also called Fulling-Davies-Unruh effect) can also be observed in the present scheme as a result of strong nonadiabaticity. In the conventional Unruh effect, the atom is uniformly accelerated in a Minkowski vacuum [15–17]. The atom feels a thermal field environment expressed as a Boltzmann factor $e^{-2\pi\omega/\alpha}$, where $\alpha = a/c$, a is the acceleration, α is called the acceleration rate, and ω is the atomic energy frequency. The factor is as tiny as 10^{-200}, which restrains the observation of this effect in experiment. In a novel scheme, Scully and collaborators demonstrate that this factor can be increased to 10^{-3} via nonadiabatic effects in cavity QED systems [18–20]. However, due to the screening effect arising from the thick cavity wall, it may be difficult to obtain uniform acceleration. At present no scheme seems to exist where Unruh effect can be observed under realistic conditions. Our present model provides a practical platform to realize strong nonadiabatic effect via GPs to enhance the Boltzmann factor to almost equal to unity for two-level quantum emitters moving at a speed just about $10^{-4}c$. When the emitter transition frequency is resonant with the GPs, i.e., the emitter can absorb the GP strongly, the Boltzmann factor can still reach a large value, equal to $\alpha/(4\alpha_c\omega_F S_p^2)$, where S_p is a constant dependent on the initial position of the emitter and ω_F

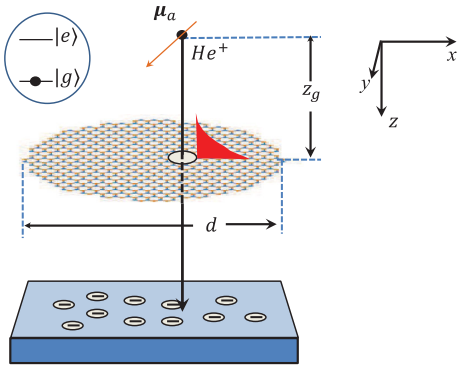

FIG. 1. A two-level emitter, such as a He^+, is attracted by a gate to pass through a graphene nanosheet along z direction. The starting point of acceleration is the origin point and the graphene nanosheet is paced in the $z = z_g$ plane.

is the Fermi frequency of the graphene. This provides a realistic system to observe the important effect with current technologies.

Model.—The model is schematically shown in Fig. 1. A two-level quantum emitter in its initial state $|g\rangle$ passes through the graphene nanosheet along the z axis. In the process, a GP as well as the quantum emitter are simultaneously excited. This can be understood as the manifestation of the dynamical Casimir effect. Our model therefore provides a platform to observe this important effect. In a special case that the quantum emitter is accelerated with a uniform acceleration, the quantum emitter feels a thermal environment with an effective temperature which is dependent on the acceleration. As a consequence, the model can be used to simulate the Unruh effect. Thus, under appropriate conditions, both the elusive dynamical Casimir effect and Unruh effect can be observed. In the case when the quantum emitter is assumed to undergo uniform acceleration, the emitter, such as He^+ ion, can be attracted by the gate. The quantum emitter has a ground level $|g\rangle$ and an excited level $|e\rangle$. To match the energies of low loss GPs from meV to 200 meV, the emitter can be firstly excited to a level with high principal quantum number, such as $n = 9$–16 in He^+. The vibration energy levels of the molecule can also be candidates of the excited and ground levels. As the passage time through the graphene nanosheet is on the order $10^{-11} - 10^{-10}$ s, the emitter can be considered to be a two-level system for the whole duration. The system is placed in vacuum. The accelerating electric field strength E_S can reach 10^8 V/m. The corresponding acceleration a can be as large as $\sim 2.5 \times 10^{15}$ m/s^2. The emitter's trajectory is given by Rindler transformation as $t(\tau) = t_0 + (1/\alpha)\sinh(\alpha\tau)$, $z(\tau) = (c/\alpha)[\cosh(\alpha\tau) - 1]$ [21–23], where τ is the proper time and t is the lab time. The emitter starts to be accelerated at t_0. Here t_0 is set to be 0.

A circular graphene nanosheet of diameter d is suspended at position z_g. The surface conductivity of the graphene can be expressed as [11]

$$\sigma(\omega_p) = \frac{ie^2 E_F}{\pi\hbar^2(\omega_p + i\gamma)} + \frac{e^2}{4\hbar}\left[\Theta(\hbar\omega_p - 2E_F) + \frac{i}{\pi}\ln\left|\frac{\hbar\omega_p - 2E_F}{\hbar\omega_p + 2E_F}\right|\right], \quad (1)$$

under the random phase approximation. Here, E_F is the Fermi level, e is the electronic charge, and $\Theta(x)$ is a Heaviside step function, i.e., $\Theta(x) = 1$ for $x \geq 0$ and $\Theta(x) = 0$ for $x < 0$. γ denotes the momentum relaxation rate and can be expressed as $\gamma = ev_F^2/\mu E_F$. Here, μ is the mobility of the graphene charge carriers, whose value can reach $10^4 - 10^6$ cm^2 V^{-1} s^{-1}. By adjusting the Fermi level, the GP wave number on a monolayer graphene can be expressed as $k_p = k_0\sqrt{1 - [2/\sigma(\omega_p)]^2\varepsilon_0/\mu_0}$, where k_0 is the vacuum wave number, ε_0 and μ_0 are the vacuum permittivity and permeability. The GPs on a graphene nanoparticle have also been widely investigated [8–10]. If $E_F = 8$ meV and the graphene nanosheet is a circular disk with diameter $d = 280$ nm, the $m = 1$ eigenmode of the graphene nanosheet has a resonant frequency $\hbar\omega_p \approx 10$ meV and plasmonic wave number $k_p \approx 140k_0$ [8]. The wave number component perpendicular to the graphene nanosheet can be expressed as $i\beta = \sqrt{k_0^2 - k_p^2}$. As k_p is about 2 orders lager than k_0, β has almost the same amplitude as k_p.

The electric field distribution has the following form (such as for the $m = 1$ eigenmode) [8,24],

$$E = \begin{cases} E_0^p e^{-\beta[z_g - z(\tau)]} & z(\tau) \leq z_g \\ E_0^p e^{\beta[z_g - z(\tau)]} & z(\tau) > z_g, \end{cases} \quad (2)$$

for the electric field parallel to the graphene nanosheet. Here, E_0^p is the electric field on the graphene layer. In the emitter's rest frame, the parallel component of the electric field E' felt by the emitter is related to the electric field in the lab frame as $E' = \sqrt{(c - v)/(c + v)}E$. Here, the velocity $v = c\tanh(\alpha\tau)$, and we have $E' = Ee^{-\alpha\tau}$.

Next we examine the case when the electric field is perpendicular to the graphene nanosheet. In this case, $E' = E$. The electric field can be expressed as (for example, for the $m = 0$ or $m = 1$ mode) [8,24]

$$E = \begin{cases} E_0^n e^{-\beta[z_g - z(\tau)]} & z(\tau) < z_g \\ -E_0^n e^{\beta[z_g - z(\tau)]} & z(\tau) > z_g. \end{cases} \quad (3)$$

For the sake of comparison, we choose $|E_0^p| = |E_0^n| = E_0$. Here, $E_0 \approx \sqrt{2\pi\hbar\omega_p\beta/(3S_0\varepsilon_0)}$ and S_0 is the area of the graphene nanosheet [24]. The electric field strength can reach $(1 - 10) \times 10^5$ V/m, leading to strong interaction with the emitter. According to Eq. (3), the vertical electric field directions on the two sides of the graphene layer are

opposite. This means that the coupling strength $g(\tau) = E'\mu_a/\hbar$ has opposite values when the emitter with dipole perpendicular to the graphene layer passes through the nanosheet. Here μ_a is the dipole moment.

Under single mode coupling and dipole approximations, the Hamiltonian of the system can be expressed as [25,26]

$$H = \hbar\omega_p\hat{\alpha}^\dagger\hat{\alpha} + \hbar\omega\hat{\sigma}_z - \hbar g(\tau)(\hat{\alpha}^\dagger + \hat{\alpha})(\hat{\sigma}^+ + \hat{\sigma}). \quad (4)$$

Here $\hat{\alpha}^\dagger$ and $\hat{\alpha}$ are the plasmon creation and annihilation operators, $\hat{\sigma}_z = |e\rangle\langle e|$, $\hat{\sigma}^\dagger = |e\rangle\langle g|$, and $\hat{\sigma} = |g\rangle\langle e|$ are the emitter's raising and lowering operators. The probability of excitation of the emitter with the simultaneous emission of a photon is due to the counterrotating term $\hat{a}^\dagger\hat{\sigma}^\dagger$ in the interaction Hamiltonian. The probability of this event is $P_e = (1/\hbar^2)|\int_{\tau_i}^{\tau_f} d\tau\langle 1, e|H|0, g\rangle|^2 = |I_e|^2$. Here τ_i and τ_f are the beginning and end times of the acceleration. The time τ_g when the emitter arrives at the graphene nanosheet is $\tau_g = \text{arcosh}(1 + \alpha z_g/c)/\alpha$. We note that the strength of the GPs decays exponentially from the graphene layer and the GPs can exist only in the vicinity of the layer with range $z_c = |z(\tau) - z_g| < 1/\beta$. The corresponding time of the emitter passing through this range is about $2\sqrt{z_c/(c\alpha)}$, which satisfies $\alpha\tau \to 0$ if z_g is set to be comparable with z_c.

It follows that, for the dipole parallel to the graphene nonosheet, I_e^p is given by

$$I_e^p = \int_0^{\tau_g} g_0 e^{\beta\alpha c\tau^2/2 - \beta z_g - \alpha\tau + i(\omega_p+\omega)\tau} d\tau + \int_{\tau_g}^{\tau_f} g_0 e^{\beta z_g - \beta\alpha c\tau^2/2 - \alpha\tau + i(\omega_p+\omega)\tau} d\tau. \quad (5)$$

Here we have set $\tau_i = 0$ and $g_0 = E_0\mu_a/\hbar$. As $\alpha \ll 1/\tau$, we can ignore $\alpha\tau$ terms in the exponent. On integrating by parts,

$$I_e^p = -\int_0^{\tau_g} g_0\beta\alpha c\tau \frac{e^{\beta\alpha c\tau^2/2 - \beta z_g + i(\omega_p+\omega)\tau}}{i(\omega_p+\omega)} d\tau + \int_{\tau_g}^{\tau_f} g_0\beta\alpha c\tau \frac{e^{\beta z_g - \beta\alpha c\tau^2/2 + i(\omega_p+\omega)\tau}}{i(\omega_p+\omega)} d\tau. \quad (6)$$

The profile of the integrand functions have quasi-Gaussian form with center at τ_g. The functions oscillate strongly with period $\omega_p + \omega$. The stationary point is far away from the integration path, which means the excitation probability is low.

Following the same procedure as just discussed, we obtain the corresponding I_e^n when the dipole is perpendicular to the graphene nanosheet:

$$I_e^n = \frac{2g_0 e^{i(\omega_p+\omega)\tau_g}}{i(\omega_p+\omega)} - \int_0^{\tau_g} g_0\beta\alpha c\tau \frac{e^{\beta\alpha c\tau^2/2 - \beta z_g + i(\omega_p+\omega)\tau}}{i(\omega_p+\omega)} d\tau + \int_{\tau_g}^{\tau_f} g_0\beta\alpha c\tau \frac{e^{\beta z_g - \beta\alpha c\tau^2/2 + i(\omega_p+\omega)\tau}}{i(\omega_p+\omega)} d\tau. \quad (7)$$

Compared to the results for the dipole parallel to the sheet, we have an additional contribution proportional to the coupling strength g_0, which results from the flipping of the interaction strength and represents a strong nonadiabatic effect of the emitter evolution; i.e., $d[g(\tau)/(\omega_p+\omega)]/d\tau \gg g_0$. When the emitter arrives at the graphene nanosheet, the dressed ground state of the system is $|\varphi\rangle_g^d = |0, g\rangle + g_0/(\omega_p+\omega)|1, e\rangle$, while when the emitter passes through the graphene nanosheet, the dressed excited state is $|\varphi\rangle_e^d = |1, e\rangle + g_0/(\omega_p+\omega)|0, g\rangle$. The abrupt nonadiabatic change of the dressed eigenstates yields a real GP exciting probability $|\langle\varphi|_e^d|\varphi\rangle_g^d|^2 = 4g_0^2/(\omega_p+\omega)^2$.

For the transition from the states with principal quantum number $n = 9$–16 in He^+, the dipole moments can be much larger than those given in Fig. 2. Meanwhile, the GPs can be made more localized by controlling the diameter as well as the Fermi level of the graphene nanosheet. The coupling strength g_0 can reach 10^{12}–10^{13}/s [8] and the corresponding excitation probability can therefore become as large as 0.01–1. In Fig. 2, the excitation probabilities are presented under different conditions. It is shown that the nonadiabatic effect induced excitation dominates the total probability P_e^n.

We also note that, due to the strong field localization, weak nonadiabatic effect happens, $d[g(\tau)/(\omega_p+\omega)]/d\tau \approx g_0\beta\alpha c\tau_g/(\omega_p+\omega) \approx 10^{-2}g_0$, for the dipole parallel to the graphene nanosheet, and P_e^p also has small value. Large α yields large speed, i.e., $\beta\alpha c\tau_g$, of the emitter while passing through the localized GP. This induces stronger nonadiabatic effect and larger excitation probability P_e^p. In a real

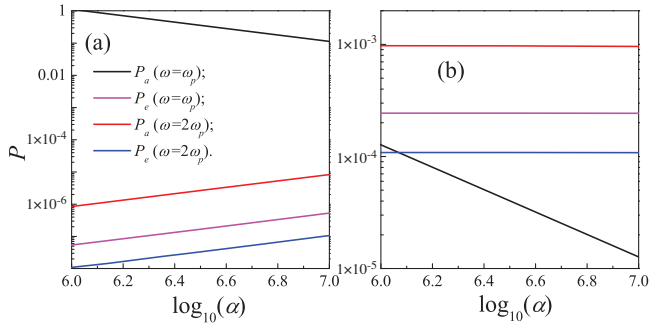

FIG. 2. The excitation P_e and absorption P_a probabilities as a function of the acceleration rate. In (a) and (b), the dipoles are parallel and perpendicular to graphene nanosheet, respectively. $\hbar\omega_p = 10$ meV, $\beta = 140k_0$, $z_g = 15\pi/\beta$, $E_0 = 2.5 \times 10^5$ V/m, and the dipole moment $\mu_a = 10^{-28}$ Cm.

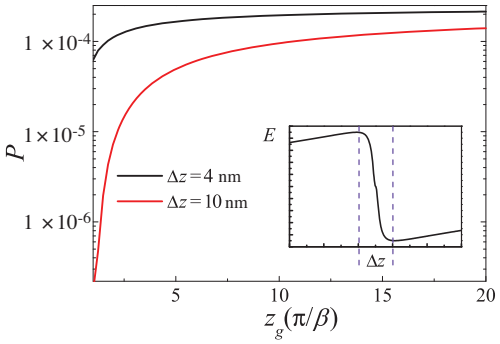

FIG. 3. The excitation probability as a function of the z_g with different hole size. The acceleration rate $\alpha = 3.3 \times 10^6/\mathrm{s}$. The other parameters are the same as Fig. 2. The inset is the field distribution along the emitter trajectory.

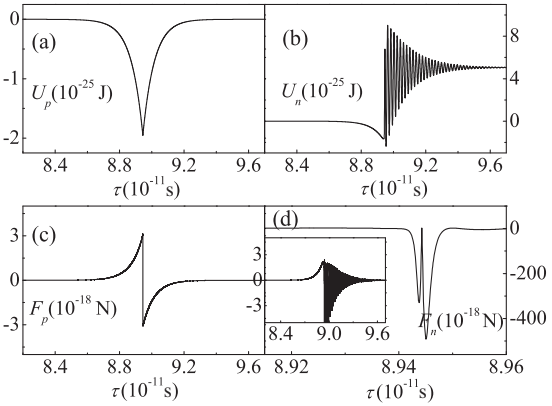

FIG. 4. (a),(b) Casimir-potential energy for the emitter's dipole parallel and perpendicular to the graphene nanosheet. (c),(d) Corresponding Casimir-Polder force. The simulation is based on the field distribution shown in Fig. S1 in the Supplemental Material [28]. Here $\alpha = 3.3 \times 10^6/\mathrm{s}$, $z_g = 10\pi/\beta$, and $\Delta z = 6$ nm.

experiment, a hole on the graphene nanosheet may be required to pass the emitter through the graphene. This disturbs the field distribution near the graphene [10]. The field distribution depends on the parameters of the graphene nanosheet, such as the nanosheet diameter, the hole's sharp, size, and the Fermi level. We show the influence of the field defect on P_e^n in Fig. 3 and in Sec. S1 of the Supplemental Material [28]. The figure shows that the defect can really weaken the nonadiabatic process. However, if the defect size is small and the emitter's speed can be as large as $10^{-4}c$, the influence can be neglected.

The strong nonadiabatic variation of the interaction between the quantum emitter and the GPs leading to induced GP excitation actually is analogous to the dynamical Casimir effect, where the modulation frequency of the coupling strength (which is comparable with the photonic frequency) plays the same role as the oscillation frequency of the mirror. In the present model, the emitter undergoes varying coupling strength $g(\tau)$ while passing through the graphene nanosheet. $g(\tau)$ can be expanded to a series of $e^{i\Omega\tau}$ with Ω analogy to the dynamic modulation or mirror oscillation frequency in dynamical Casimir effect [13]. For the dipole parallel to the graphene nanosheet, $g(\tau)$ varies slowly and Ω mainly distributes in the low frequency region. As a consequence, almost no dynamical Casimir effect happens. However, for the dipole perpendicular to the graphene nanosheet, $g(\tau)$ varies sharply. The Fourier expansion frequencies Ω can reach very large value and strong dynamical Casimir effect appears. As shown in Fig. 3, if $\Delta\tau$ is large, i.e., Δz is large and the emitter's speed is small, effective Ω moves to small value and the dynamical Casimir effect is absent. It should also be noted that the excitation of the GPs needs the quantum emitter to pass the graphene nanosheet with uniform velocity. This means the acceleration device in Fig. 1 is not required and the experimental setup is much simpler. If the quantum emitter has a constant speed, it moves in a Minkowski space and the corresponding trajectory satisfies Lorentz transformation.

In order to understand where the energy comes from to excite the GP and the emitter simultaneously, we look at the plots in Fig. 4. During the passage of the emitter through the graphene nanosheet, attractive and repulse forces, called Casimir-Polder force, act on the emitter (see Sec. S2 of the Supplemental Material [28]). In case the dipole is parallel to the graphene nanosheet, the dressed ground state evolves from $|\varphi\rangle_g = |0, g\rangle$ to $|\varphi\rangle_g^d$ almost adiabatically before the emitter arrives at the graphene nanosheet. The Casimir-Polder force is attractive [30,31]. After the emitter passes the sheet, the system evolves from $|\varphi\rangle_g^d$ to $|\varphi\rangle_g$. The Casimir-Polder force is an attractive force again. The total work by the Casimir-Polder force, i.e., the energy loss of the emitter, is small [see Figs. 4(a) and 4(c)]. However, for the dipole perpendicular to the graphene nanosheet, the excited GP brings additional force on the emitter. In the region where the electric direction flips, the force is huge and dependent on the gradient of the field strength distribution. The total work applied on the emitter is large [see Sec. S2 of the Supplemental Material [28] and Figs. 4(b) and 4(d)] and is equal to the energy that excites the emitter and GP simultaneously. This means that the total energy is conserved during the whole process.

Next we consider the simulation of Unruh effect in our model. After the GP is excited, the GP can be absorbed by the emitter. The absorption probability can be expressed as $P_a = |\int_{\tau_i}^{\tau_f} d\tau g(\tau) e^{-i\omega_p t(\tau) + i\omega\tau}|^2$. The corresponding expressions are the same as Eqs. (5)–(7) but with ω_p replaced by $-\omega_p$. In Fig. 2, we plot the absorption probability (see Sec. S3 of the Supplemental Material [28]). For a beam accelerated emitters passing through the graphene nanosheet at some position between the center and edge of the circular graphene nanosheet, where the $m = 1$ mode can interact with the dipoles parallel and perpendicular to the graphene nanosheet simultaneously [8],

the GPs satisfy thermal field distribution with temperature $T = \hbar\omega_p/k_B \ln[(P_a + \gamma/r_a)/P_e]$. For a special case that $\omega = \omega_p$ and $E_0^p = E_0^n$, the Boltzmann factor of GPs has the expression $P_e/P_a = \beta\alpha c/2\omega_p^2 S_p^2 = \alpha/4\alpha_c\omega_F S_p^2$. Here we have set $\beta \approx k_p \approx \hbar\omega_p k_0/2\alpha_c E_F$. $\omega_F = E_F/\hbar$. Since $4\omega_F S_p^2$ is on the order of ω, this factor has a $1/\alpha_c$ increase compared to that in Ref. [18]. It should be noted that the emitter transition frequency is resonant with the GP here. Under this condition, the absorption probability P_a in Ref. [18] could be huge and decreases the Boltzmann factor strongly.

We address the following question: How can we achieve uniform acceleration that is required to observe Unruh effect? For this purpose, the emitter needs to be charged. Meanwhile, the graphene nanosheet is suspended like the model in Refs. [2,3] but with supporting materials, i.e., drain and source, replaced by dielectric with low relative permittivity. The graphene nanosheet is kept neutral and the screening effect from the graphene layer and supporting material can be neglected. In Sec. S4 of the Supplemental Material [28], it is shown that the excitation probability by a moving charged particle can be neglected if the particle has a low speed, as in the present model. During the whole process, the electric field of the GPs $E_0 \ll E_S$. Meanwhile, the average Casimir-Polder force applied on the emitter satisfies $F\Delta z \sim \hbar g_0^2/(\omega_p + \omega)$ and the force, as shown in Fig. 4(d), is about 10^{-4} times the static force. This means that the emitter can be assumed to be undergoing uniform acceleration.

Compared to the surface plasmons on other plasmonic structure, such as a metal slab, the plasmonic frequency on graphene is low, which leads to a large excitation probability P_e as shown in Eq. (7). The single atom thickness of graphene allows a strong nonadiabatic environment and the weak screening effect guarantees uniform acceleration. The stronger field localization ability and lower loss induce strong coupling strength between the emitter and the long-lived GPs. In a recent experiment, long lifetime GPs have been achieved in high-quality graphene [32,33]. Meanwhile, for a dipole mode of the graphene nanosheet ($m = 1$ mode), the GPs can be radiated to far field with certain probability and subsequently observed easily [34,35]. These make our proposal experimentally feasible with the current technologies.

Conclusion.—In this Letter, we investigated the GP's excitation by passing quantum emitters in ground state through graphene nanosheet. The field distribution of the GP around the graphene nanosheet can construct a strong nonadiabatic environment for the evolution of the emitter and GP, which can excite the emitter with simultaneous emission of a GP with large probability. The energy comes from the loss of the emitter's kinetic energy. The process can be understood by dynamical Casimir effect but with low speed. For a beam of accelerated emitters passing through the graphene nanosheet, the excited GP density becomes a thermal distribution with a high temperature. The present model provides a promising platform to observe the dynamical Casimir effect as well as a simulation of the Unruh effect.

This work is supported by National Natural Science Foundations of China (11804219) and a grant from King Abdulaziz City for Science and Technology (KACST).

*zengxdgood@shu.edu.cn
†zubairy@physics.tamu.edu

[1] A. K. Geim and K. S. Novoselov, The rise of graphene, Nat. Mater. **6**, 183 (2007).
[2] A. H. Castro Neto, F. Guinea, N. M. R. Peres, K. S. Novoselov, and A. K. Geim, The electronic properties of graphene, Rev. Mod. Phys. **81**, 109 (2009).
[3] K. I. Bolotina, K. J. Sikesb, Z. Jiangad, M. Klimac, G. Fudenberga, J. Honec, P. Kima, and H. L. Stormer, Ultrahigh electron mobility in suspended graphene, Solid State Commun. **146**, 351 (2008).
[4] J. Chen, M. Badioli, and P. Alonso-González, S. Thongrattanasiri, F. Huth, J. Osmond, M. Spasenović, A. Centeno, A. Pesquera, P. Godignon, A. Z. Elorza, N. Camara, F. J. Garcia de Abajo, R. Hillenbrand, and F. H. L. Koppens, Optical nano-imaging of gate-tunable graphene plasmons, Nature (London) **487**, 77 (2012).
[5] Z. Fei, A. S. Rodin, G. O. Andreev, W. Bao, A. S. McLeod, M. Wagner, L. M. Zhang, Z. Zhao, M. Thiemens, G. Dominguez, M. M. Fogler, A. H. Castro Neto, C. N. Lau, F. Keilmann, and D. N. Basov, Gate-tuning of graphene plasmons revealed by infrared nano-imaging, Nature (London) **487**, 82 (2012).
[6] X. D. Zeng, M. Al-Amri, and M. S. Zubairy, Nanometer-scale microscopy via graphene plasmons, Phys. Rev. B **90**, 235418 (2014).
[7] Z. Fang, S. Thongrattanasiri, A. Schlather, Z. Liu, L. Ma, Y. Wang, P. M. Ajayan, P. Nordlander, N. J. Halas, and F. J. Garcia de Abajo, Gated tunability and hybridization of localized plasmons in nanostructured graphene, ACS Nano **7**, 2388 (2013).
[8] F. H. L. Koppens, D. E. Chang, and F. J. Garcia de Abajo, Graphene plasmonics: A platform for strong light-matter interactions, Nano Lett. **11**, 3370 (2011).
[9] A. N. Grigorenko, M. Polini, and K. S. Novoselov, Graphene plasmonics, Nat. Photonics **6**, 749 (2012).
[10] R. Yu, J. D. Cox, J. R. M. Saavedra, and J. Garcia de Abajo, Analytical modeling of graphene plasmons, ACS Photonics **4**, 3106 (2017).
[11] M. Jablan, H. Buljan, and M. Soljačič, Plasmonics in graphene at infrared frequencies, Phys. Rev. B **80**, 245435 (2009).
[12] M. Antezza, C. Braggio, G. Carugno, A. Noto, R. Passante, L. Rizzuto, G. Ruoso, and S. Spagnolo, Optomechanical Rydberg-Atom Excitation via Dynamic Casimir-Polder Coupling, Phys. Rev. Lett. **113**, 023601 (2014).
[13] C. M. Wilson, G. Johansson, A. Pourkabirian, M. Simoen, J. R. Johansson, T. Duty, F. Nori, and P. Delsing, Observation of the dynamical Casimir effect in a superconducting circuit, Nature (London) **479**, 376 (2011).

[14] P. Lähteenmäki, G. S. Paraoanu, J. Hassel, and P. J. Hakonen, Dynamical Casimir effect in a Josephson metamaterial, Proc. Natl. Acad. Sci. U.S.A. **110**, 4234 (2013).
[15] W. G. Unruh, Notes on black hole evaporation, Phys. Rev. D **14**, 870 (1976).
[16] S. A. Fulling, Nonuniqueness of canonical field quantization in Riemannian space-time, Phys. Rev. D **7**, 2850 (1973).
[17] W. G. Unruh and R. M. Wald, What happens when an accelerating observer detects a Rindler particle, Phys. Rev. D **29**, 1047 (1984).
[18] M. O. Scully, V. V. Kocharovsky, A. Belyanin, E. Fry, and F. Capasso, Enhancing Acceleration Radiation from Ground-State Atoms via Cavity Quantum Electrodynamics, Phys. Rev. Lett. **91**, 243004 (2003).
[19] A. Belyanin, V. V. Kocharovsky, F. Capasso, E. Fry, M. S. Zubairy, and M. O. Scully, Quantum electrodynamics of accelerated atoms in free space and in cavities, Phys. Rev. A **74**, 023807 (2006).
[20] M. O. Scully, S. Fulling, D. Lee, D. Page, W. Schleich, and A. A. Svidzinsky, Quantum optics approach to radiation from atoms falling into a black hole, Proc. Natl. Acad. Sci. U.S.A. **115**, 8131 (2018).
[21] P. Davies, Scalar production in Schwarzschild and Rindler metrics, J. Phys. A **8**, 609 (1975).
[22] N. Birrell and P. Davies, *Quantum Fields in Curved Spacetime* (Cambridge University Press, Cambridge, England, 1982).
[23] V. L. Ginzburg and V. P. Frolov, Vacuum in a homogeneous gravitational field and excitation of a uniformly accelerated detector, Sov. Phys. Usp. **30**, 1073 (1987).
[24] V. Apalkov and M. I. Stockman, Proposed graphene nanospaser, Light Sci. Appl. **3**, e191 (2014).
[25] M. O. Scully and M. S. Zubairy, *Quantum Optics* (Cambridge University Press, Cambridge, England, 1997).
[26] For a graphene nanosheet, the dependence of the coupling strength on the frequency can be denoted by a Lorentz function as $g_0^2(\omega_p) = g_0^2\gamma^2/4[(\omega_p - \omega_r)^2 + \gamma^2/4]$ [27]. Here, ω_r is the resonant frequency. In this case, we need to do integration on the frequency to consider the contributions of different frequencies. By using residue theorem, there will be a decay component $e^{-\gamma\tau}$ in the excitation probability.
[27] M. Jablan and D. E. Chang, Multiplasmon Absorption in Graphene, Phys. Rev. Lett. **114**, 236801 (2015).
[28] See Supplemental Material at http://link.aps.org/supplemental/10.1103/PhysRevLett.126.117401 for additional discussions about Casimir-Polder force, GPs excitation by a moving ion, and other discussions, which includes Ref. [29].
[29] F. J. Garcia de Abajo, Multiple excitation of confined graphene plasmons by single free electrons, ACS Nano **7**, 11409 (2013).
[30] H. R. Haakh, C. Henkel, S. Spagnolo, L. Rizzuto, and R. Passante, Dynamical Casimir-Polder interaction between an atom and surface plasmons, Phys. Rev. A **89**, 022509 (2014).
[31] S. Y. Buhmann and D. G. Welsh, Dispersion forces in macroscopic quantum electrodynamics, Prog. Quantum Electron. **31**, 51 (2007).
[32] A. Woessner, M. B. Lundeberg, Y. Gao, A. Principi, and P. Alonso-González, M. Carrega, K. Watanabe, T. Taniguchi, G. Vignale, M. Polini, J. Hone, R. Hillenbrand, and F. H. L. Koppens, Highly confined low-loss plasmons in graphene-boron nitride heterostructures, Nat. Mater. **14**, 421 (2015).
[33] G. X. Ni, A. S. McLeod, Z. Sun, L. Wang, L. Xiong, K. W. Post, S. S. Sunku, B.-Y. Jiang, J. Hone, C. R. Dean, M. M. Fogler, and D. N. Basov, Fundamental limits to graphene plasmonics, Nature (London) **557**, 530 (2018).
[34] M. A. Noginov, G. Zhu, A. M. Belgrave, R. Bakker, V. M. Shalaev, E. E. Narimanov, S. Stout, E. Herz, T. Suteewong, and U. Wiesner, Demonstration of a spaser-based nanolaser, Nature (London) **460**, 1110 (2009).
[35] F. J. Garcia de Abajo, Optical excitation in electron microscopy, Rev. Mod. Phys. **82**, 209 (2010).